# Silica-Coated Magnetic Nanoparticles Activate Microglia and Induce Neurotoxic D-Serine Secretion

**Tae Hwan Shin**
Ajou University School of Medicine and Graduate School of Medicine
**Da Yeon Lee**
Ajou University School of Medicine and Graduate School of Medicine
**Balachandran Manavalan**
Ajou University School of Medicine and Graduate School of Medicine
**Shaherin Basith**
Ajou University School of Medicine and Graduate School of Medicine
**Yun-Cheol Na**
Korea Basic Science Institute
**Cheolho Yoon**
Korea Basic Science Institute Seoul Center
**Hyeon-Seong Lee**
Sunchon National University
**Man Jeong Paik**
Sunchon National University
**Gwang Lee** ( glee@ajou.ac.kr )
Ajou University School of Medicine and Graduate School of Medicine https://orcid.org/0000-0002-1299-9478

**Research article**

**Keywords:** silica-coated magnetic nanoparticles, nanotoxicity, microglia, excitotoxicity, inclusion body

**Posted Date:** March 9th, 2021

**DOI:** https://doi.org/10.21203/rs.3.rs-202837/v2



**Version of Record:** A version of this preprint was published at Particle and Fibre Toxicology on August 12th, 2021. See the published version at https://doi.org/10.1186/s12989-021-00420-3.

## Abstract

# Background

Nanoparticles have been studied for brain imaging, diagnosis, and drug delivery owing to their versatile properties due to their small sizes. However, there are growing concerns that nanoparticles may exert toxic effects in the brain. In this study, we assessed direct nanotoxicity on microglia, the resident macrophages of the central nervous system, and indirect toxicity on neuronal cells exerted by silica-coated magnetic nanoparticles containing rhodamine B isothiocyanate dye [MNPs@$SiO_2$(RITC)].

# Methods

We investigated MNPs@$SiO_2$(RITC)-induced biological changes in BV2 murine microglial cells via RNA-sequencing-based transcriptome analysis and gas chromatography-mass spectrometry-based intracellular and extracellular amino acid profiling. Morphological changes were analyzed by transmission electron microscopy. Indirect effects of MNPs@$SiO_2$(RITC) on neuronal cells were assessed by Transwell-based coculture with MNPs@$SiO_2$(RITC)-treated microglia. MNPs@$SiO_2$(RITC)-induced biological changes in the mouse brain *in vivo* were examined by immunohistochemical analysis.

# Results

BV2 murine microglial cells were morphologically activated and the expression of Iba1, an activation marker protein, was increased after MNPs@$SiO_2$(RITC) treatment. transmission electron microscopy analysis revealed lysosomal accumulation of MNPs@$SiO_2$(RITC) and the formation of vesicle-like structures in MNPs@$SiO_2$(RITC)-treated BV2 cells. The expression of several genes related to metabolism and inflammation were altered in 0.1 μg/μl MNPs@$SiO_2$(RITC)-treated microglia when compared with that in non-treated (control) and 0.01 μg/μl MNPs@$SiO_2$(RITC)-treated microglia. Combined transcriptome and amino acid profiling analyses revealed that the transport of serine family amino acids, including glycine, cysteine, and serine, was enhanced. However, only serine was increased in the growth medium of activated microglia; especially, excitotoxic d-serine secretion from primary rat microglia was the most strongly enhanced. Activated primary microglia reduced intracellular ATP levels and proteasome activity in cocultured neuronal cells, especially in primary cortical neurons, via d-serine secretion. Moreover, ubiquitinated proteins accumulated and inclusion bodies were increased in primary dopaminergic and cortical neurons cocultured with activated primary microglia. *In vivo*, MNPs@$SiO_2$(RITC), d-serine, and ubiquitin aggresomes were distributed in the MNPs@$SiO_2$(RITC)-treated mouse brain.

# Conclusions

MNPs@$SiO_2$(RITC)-induced activation of microglia triggers excitotoxicity in neurons via d-serine secretion, highlighting the importance of neurotoxicity mechanisms incurred by nanoparticle-induced microglial activation.

# Background

Nanoparticles (NPs) for drug delivery, imaging, and diagnosis to the brain have been studied due to their ultra-small sizes. Some types of NPs, such as polymeric NPs [1], gold NPs [2], zinc oxide NPs [3], quantum dots [4], and silica-coated magnetic nanoparticles containing rhodamine B isothiocyanate dye [MNPs@$SiO_2$(RITC)] [5] can cross the blood–brain barrier (BBB) through passive diffusion and endocytosis to access the brain. Accumulation of NPs in the brain is a serious concern owing to its toxic effects on CNS. Previous studies reported that NPs exposure and accumulation can induce neurodegeneration in brain by oxidative stress, deficits in motor and cognitive functions, neuronal deterioration, DNA damage by lipid peroxidation, neuroinflammatory response, microglia/astrocyte activation, and BBB damage/dysfunction [6]. In mice, MNPs@$SiO_2$(RITC) crossed the BBB without disrupting it and accumulated in the brain for longer than 4 weeks, although toxicological symptoms were not detected using conventional methods [5].

Previous studies have found that protein fibrilization is observed in Alzheimer's disease by NPs (cerium oxide particles, copolymer particles, carbon nanotubes, quantum dots) *in vitro* [7], nuclear protein aggregation by silica NPs is observed in a cellular model of Huntington's disease, and formation of intracellular cytoplasmic inclusion bodies by MNPs@$SiO_2$(RITC) in neuronal cells [8], may play a crucial role in neurodegenerative diseases. In addition, internalized metal-oxide nanoparticles in microglia-induced inflammation is a common factor in many neurodegenerative diseases [9]. However, studies related to neuro-nanotoxicity is very limited and its research area is still in infancy.

Microglia are resident macrophages which account for 5–20% of the total brain cells. They are uniformly distributed [10]. and activated by internalized NPs [11]. Upon activation by NPs, microglia secrete large amounts of ROS and nitric oxide (NO) and release various cytotoxic substances. The secreted substances can damage neurons and trigger neuronal death. For example, activated microglia impair neurons through *N*-methyl-d-aspartate (NMDA) receptor-mediated excitotoxicity by NMDA, polyamines, d-serine, and proteinogenic amino acid, such as glutamate and glycine [12, 13]. However, the toxicological mechanisms of activated microglia by NPs are not clearly understood.

There are also few limitations in the evaluation of nanotoxicity using conventional methods due to its delicate complexities. Therefore, omics analyses have been used in the assessment of nanotoxicity through the quantification of gene expression, proteins, and metabolites for interpreting complex biological events and finding relationships between molecules and phenomena [14, 15]. Thus, integrated omics is indispensable to compensate for their related weaknesses and comprehensive analysis of nanotoxicity.

We investigated MNPs@$SiO_2$(RITC)-induced biological changes in microglia by transcriptome analysis combined with amino acid profiling. Additionally, we examined the indirect effects of the MNPs@$SiO_2$(RITC) on neuronal cells by co-culturing with MNPs@$SiO_2$(RITC)-treated microglia. Finally, we validated MNPs@$SiO_2$(RITC)-induced biological changes in the mouse brain *in vivo* through immunohistochemical analysis.

# Methods

### MNPs@$SiO_2$(RITC) and silica NPs

MNPs@$SiO_2$(RITC) composed of a ~9-nm cobalt ferrite core ($CoFe_2O_3$) and an RITC-encompassed silica shell [16] were purchased from Biterials (Seoul, South Korea). The MNPs@$SiO_2$(RITC) were determined to be 50 nm in diameter using transmission electron microscopy (TEM) (Supplementary Fig. 1), and the MNPs@$SiO_2$(RITC) had a zeta potential between −40 and −30 mV [16, 17]. X-ray diffraction (XRD) using a High-Power X-Ray Diffractometer (Ultima III, Rigaku, Japan) confirmed the structure of the MNPs@$SiO_2$(RITC), which showed specific patterns of $CoFe_2O_4$: (220) at 30°, (311) at 36°, (400) at 44°, (511) at 57°, and (440) at 64°. The broad peak between 20° and 40° indicated amorphous silica beads (Supplementary Fig. 2). The biological changes of HEK293 cells were induced by the shell (silica) rather than the cobalt ferrite core of MNPs@$SiO_2$(RITC) [8, 18-22]. MNPs@$SiO_2$(RITC) uptake was plateaued at 0.1 μg/μl MNPs@$SiO_2$(RITC) treatment and cell viabilities of BV2 cell line and primary rat microglia were ~80% reduced at 1.0 μg/μl MNPs@$SiO_2$(RITC) treatment (data not shown). Thus, the MNPs@$SiO_2$(RITC) treatment dose to microglia was determined as 0.01 to 0.1 μg/μl in this study.

### Primary cell isolation and cell culture

Primary cortical, dopaminergic neurons, and microglia were isolated from Sprague–Dawley rats (1 day pups). Briefly, rat brains were separated into cortex and midbrain and homogenized in Minimum Essential Medium (MEM, Gibco, NY, USA). The cell fractions were cultured in dishes containing MEM supplemented with 10% fetal bovine serum (Gibco, NY, USA), 100 units/ml penicillin, and 100 ng/μl streptomycin (Gibco, NY, USA) in a humidified 5% $CO_2$ chamber at 37°C. Primary rat microglia were isolated using the “shaking off” method [23]. The purity of the primary neuronal cells was verified based on specific marker protein expression: neuronal nuclei (NeuN) for cortical neuronal cells and tyrosine hydrolase (TH) for dopaminergic neuronal cells. The purity of the primary rat microglia was verified by flow cytometry after staining with a specific antibody (CD11b/c, integrin αM; clone OX-42, Santa Cruz, CA, USA) (Supplementary Fig. 3).

### Immunocytochemistry

After MNPs@$SiO_2$(RITC) treatment or coculture on cover slips, cells were fixed in Cytofix buffer (BD Biosciences, CA, USA) at 4°C for 30 min. PBS containing 2% bovine serum albumin and 0.1% Triton-X100 (Sigma-Aldrich, MO, USA) was used for blocking the cover slips. The cells were then incubated with anti-

Iba1 goat polyclonal antibody (Novus biologicals, CO, USA), anti-d-serine rabbit polyclonal antibody (1:200, Abcam, Cambridge, UK), anti-vesicle-associated membrane protein 2 (VAMP2) mouse polyclonal antibody (1:200, GeneTex, CA, USA), anti- neuropeptide Y (NPY) mouse polyclonal antibody (1:200, GeneTex, CA, USA), anti-ubiquitin rabbit polyclonal antibody (1:200, Santa Cruz, CA, USA), and anti-alpha synuclein monoclonal antibody (1:200, BD Biosciences, CA, USA) diluted in blocking buffer at 4°C for 12 h. After three washes with PBS containing 0.1% Triton X-100, they were incubated with Alexa Fluor 488-, 547-, and 647-conjugated secondary antibodies (1:200, Invitrogen, CA, USA) at room temperature (RT) for 1 h. The labeled cells were washed thrice with PBS containing 0.1% Triton X-100 and incubated with PBS containing 10 μg/ml Hoechst 33342 at RT for 10 min. After three washes with PBS, the cover slips were mounted onto slides using Prolong Gold Antifade mounting medium (Molecular Probes, OR, USA). Fluorescence images were taken using a slide scanner (Axioscan Z1, Carl Zeiss Microscopy GmbH, Jena, Germany) or by high-resolution confocal microscopy (Nikon A1, Nikon, Tokyo, Japan) at the 3D immune system imaging core facility of Ajou University. To quantify inclusion bodies, total cells were counted using ImageJ (NIH Image, Bethesda, MD) and the frequency of aggresome-containing cells was calculated.

## TEM

To analyze ultrastructural changes, Karnovsky's fixative (Sigma-Aldrich, MO, USA) was used for MNPs@$SiO_2$(RITC)-treated BV2 cells fixation at 4°C for 12 h. After fixation, samples were washed with 0.1 M cacodylate buffer (pH 7.4). Cacodylate buffer (0.1 M) with osmium tetroxide [1% (v/v), Polysciences, PA, USA] was used for post-fixation at RT for 2 h. The samples were dehydrated with graded ethanol solutions (50%–100%), infiltrated with propylene oxide, and embedded in Epon (Polysciences, PA, USA). The samples were incubated at 35°C for 6 h, 45°C for 12 h, and 60°C for 24 h. The blocks were sectioned using an ultramicrotome (Reichert-Jung, Bayreuth, Germany). The sections were double-stained with 6% uranyl acetate (Electron Microscopy Sciences, PA, USA) for 20 min and lead citric acid for 10 min (Thermo Fisher Scientific, CA, USA) for contrast. Images were obtained using a SIGMA500 transmission electron microscope (Carl Zeiss Microscopy GmbH, Jena, Germany) at the 3D immune system imaging core facility of Ajou University. Particle number, vesicle size, mitochondria number, and size were analyzed using the Zen blue 2.3 (Carl Zeiss Microscopy GmbH, Jena, Germany) image analysis module.

## Inductively coupled plasma mass spectrometry (ICP-MS)

MNPs@$SiO_2$(RITC) in BV2 were quantified by ICP-MS (7700, Agilent, Japan) as reported [16]. Briefly, BV2 cells were incubated with 0, 0.01, or 0.1 μg/μl MNPs@$SiO_2$(RITC) for 12 h, and $5 \times 10^6$ cells were collected. The treated cells and MNPs@$SiO_2$(RITC) were digested and completely dissolved in concentrated aqua regia and hydrogen fluoride (HF). $CoFe_2O_4$, which is the core of the MNPs@$SiO_2$(RITC), contains approximately $10^{-18}$ mmol cobalt ions. Thus, the number of MNPs@$SiO_2$(RITC) in each BV2 cell was calculated.

## RNA-seq

To analyze transcriptome of 0.01, or 0.1 μg/μl MNPs@$SiO_2$(RITC) treated BV2 cells, total RNA was extracted using a TruSeq Stranded Total RNA Library Prep Kit (Illumina, CA, USA). An Agilent RNA 6000 Nano Kit (Agilent Technologies, Waldbronn, Germany) was used for analyzing RNA quality. mRNA was enriched using Magnetic beads conjugated with oligo(dT). Double-stranded cDNA was synthesized with purified mRNA after fragmentation. Sequencing adapters using a TruSeq RNA Sample Prep Kit (Illumina, CA, USA) was used for modification, including end-repair and poly(A) addition and connection, of the cDNA. The samples were isolated using Blue Pippin (Sage Science, MA, USA). cDNA library size and quality were determined using an Agilent High Sensitivity DNA Kit (Agilent Technologies, Waldbronn, Germany). The libraries were sequenced using an Illumina HiSeq2500 sequencer (Illumina, CA, USA).

### Differentially expressed gene (DEG) analysis

Low-quality reads (reads containing more than 10% skipped bases, reads containing more than 40% of bases with quality scores <20, and reads with an average quality score < 20) were filtered from the RNA-seq data using in-house scripts. Filtered reads were identified using the aligner TopHat [24]. Expression levels were calculated using Cufflinks v2.1.1 [24] and Ensembl, release 77. Multi-read-correction and fragbias- correct were used for increasing the measurement accuracy. DEGs were singled out using Cuffdiff with default parameter settings, based on $p < 0.05$.

### Gene Ontology (GO) and pathway analyses

The GO database classifies genes into functional categories and can be used to predict gene function based on Mouse Genome Informatics (MGI) data [25]. Biological changes, related with canonical pathways and functions, were analyzed using an ingenuity pathway (IPA) web-based software (Qiagen, CA, USA). A 1.5-fold change in gene expression and a 1.2-fold change in amino acid levels were used as cut-offs.

### Quantitative reverse transcription PCR (RT-qPCR)

To quantify gene expression levels of MNPs@$SiO_2$(RITC) BV2 cells, RNA extraction and cDNA construction for RT-qPCR were performed as previously study [8]. The cells were lysed using RNAzol B (Tel-Test, TX, USA). Chloroform (Sigma-Aldrich, MO, USA) and isopropyl alcohol (Sigma-Aldrich, MO, USA) were used for total RNA precipitation. Pellets were washed with 70% ethanol and the samples were dissolved in RNase-free water. The purities of samples were measured by 260 nm/230 nm and 260 nm/280 nm absorbance ratio using spectrophotometry (Eppendorf, Hamburg, Germany). cDNA was synthesized using the iScript Advanced cDNA Synthesis Kit (Bio-Rad, Hercules, CA, USA). The thermal cycle was as follows: 46°C for 20 min followed by 95°C for 1 min.

Expression levels of genes were quantified by qPCR using SsoAdvanced™ Universal SYBR® Green Supermix (Bio-Rad) and gene-specific primers (Supplementary Tables 1 and 2) on a Rotor Gene-Q system (Qiagen, CA, USA). Thermal cycles were as follows: 95°C for 5 min, followed by 50 cycles of 95°C for 5 s and 60°C for 30 s. Target gene expressions were calculated with melting curves by the $2^{-\Delta\Delta Ct}$ method.

## Gas chromatography (GC)-MS

The amino acid content in the MNPs@$SiO_2$(RITC)-treated BV2 cells and media was analyzed using GC-MS as reported previously [26]. Norvaline is used as internal standard. GC-MS was conducted in both the scan and selected-ion monitoring (SIM) modes on a 6890N gas chromatograph (Agilent Technologies, Santa Clara, CA, USA) interfaced with a 5975B mass-selective detector (70 eV, electron impact ionization mode; Agilent Technologies).

## Determination of d-serine secreted from microglia

d-Serine concentrations in the medium were determined using a d-serine colorimetric assay (Cosmo Bio, Tokyo, Japan) per the manufacturer's instructions. Briefly, medium of the MNPs@$SiO_2$(RITC) or lipopolysaccharide (LPS)-treated BV2 cells and primary rat microglia were mixed with NADH and d-serine dehydratase from *Saccharomyces cerevisiae* (DsdSC), d-serine to pyruvate converting enzyme, at 37°C for 45 min. d-serine samples incubated with nicotinamide adenine dinucleotide (NADH), but without DsdSC were used as blank. The absorbance at 340 nm was measured using a microplate reader (Molecular Devices, CA, USA). Lactate dehydrogenase (LDH) was added to the mixed samples and incubated at 37°C for 45 min. The pyruvate to lactate conversion by LDH leaded to reduction in optical density at 340 nm by NADH oxidation. The d-serine concentration was quantified by calculating the reduction absorbance at 340 nm and a d-serine standard curve.

## Liquid chromatography (LC)-MS

L- and d-Serine were purchased from Tokyo Chemical Industry (Tokyo, Japan). HPLC-grade acetonitrile, ethanol, and trifluoroacetic acid were obtained from Thermo Fisher Scientific (CA, USA). Stock solutions of l- and d-serine were prepared at 1 mg/mL in water. A standard stock solution of amino acids was diluted to 0.01–100 μg/mL for calibration. Calibration curves were plotted with seven points using the peak areas obtained for d- and l-serine versus the concentration by linear regression. The samples were centrifuged at 12,000 ´ *g* for 15 min. The supernatant was filtered through a 3-kDa filter (Millipore, Darmstadt, Germany) by centrifugation at 14,000 ´ *g* at 4°C for 30 min. The filtered aliquot was used for analysis.

Chiral dl-serine separations were performed using an Agilent 1290 infinitely LC (Agilent Technologies, Walbronn, Germany) using a CROWNPAK CR-I(+) (3.0 × 150 mm, 5 μm, Chiral Technologies) at 30°C. Mobile phase comprising acetonitrile: ethanol: water: trifluoroacetic acid (80: 15: 5: 0.5) was employed at a flow rate of 0.4 ml/min. Two microliters of sample were injected into the column using a thermostated HiP-ALS autosampler. The HPLC system was interfaced with an Agilent 6495 Q-TOF (Agilent Technologies, Walbronn, Germany) mass spectrometer. The source conditions were set to a Vcap of 3.5 kV in positive ESI mode with a sheath gas temperature of 200°C and a sheath gas flow rate of 11 ml/min. The dl-serine was detected by multiple reaction monitoring. A product ion at m/z 60 fragmented by a collision energy of 10V from the precursor ion at m/z 106 was monitored for 200 ms.

### Evaluation of neuronal cell viability in a microglia coculture system

The coculture system was set up as reported previously [27]. Briefly, neuronal cells or SH-SY5Y cells were cultured on the bottom side of a Costar Transwell plate (0.4-μm pore size; Corning, NY, USA) in a humidified 5% $CO_2$ incubator at 37°C for 24 h. Microglia in the culture inserts were treated with MNPs@$SiO_2$(RITC) or LPS for 12 h. Then, the inserts were placed in the plate and incubated for another 12 h. To measure the viability of the neuronal cells, the upper inserts were removed, and 3-(4,5-dimethylthiazol-2-yl)-5-(3-carboxymethoxyphenyl)-2-(4-sulfophenyl)-2H-tetrazolium solution (CellTiter 96® AQueous One; Promega, WI, USA) was added to each well containing the microglia. The assay plate was incubated at 37°C for 1 h. The amount of soluble formazan produced via cellular reduction was measured using a plate reader (Molecular Devices, CA, USA) at 490 nm. Values were normalized to the corresponding total protein. Images of cell morphology and density were acquired before the cell viability assay under an Axiovert 200 M fluorescence microscope (Carl Zeiss Microscopy GmbH, Jena, Germany). The excitation wavelength for the MNPs@$SiO_2$(RITC) was 530 nm.

### Measurement of the ATP concentration

The ATP concentration of the microglia cocultured neurons were determined using an ATP quantification kit (Promega, WI, USA) per the manufacturer's protocol. Briefly, the neuronal cells were detached from plate and washed with PBS. Intracellular ATP was extracted with a 1.0% trichloroacetic acid (Sigma Aldrich, MO, USA) at RT for 30 min. The extractant were mixed with a luciferin reagent/buffer mixture and then split in white 384-well plates. After 10 min of incubation at 25°C, the luminescence in each well was measured using a luminometer (LMaxII$^{384}$; Molecular Devices, CA, USA).

### Proteasome activity assay

Proteasome activity was measured using a Proteasome-Glo™ Chymotrypsin-Like Cell-Based Assay (Promega, WI, USA) per the manufacturer's protocol. Briefly, cocultured microglia were washed three times with PBS, replenished with 50 μl of serum-free medium, and left at RT. Proteasome-Glo™ cell-based buffer was mixed with luciferin detection agent and appropriate Proteasome-Glo™ substrate and incubated at RT for 30 min. Fifty-microliter aliquots of this mixture were then added to the medium in each well and incubated at RT for 10 to 15 min. Next, 90 μl of the medium containing a proteasome assay solution was transferred to corresponding wells in a white plate. Proteasome activity was determined by measuring the chymotrypsin-like activity of cellular proteasomes using the luminogenic substrate Suc-Leu-Leu-Val-Tyr-aminoluciferin in a luminometer (LMaxII$^{384}$; Molecular Devices, CA, USA) per the manufacturer's instructions.

### Evaluation of d-serine distribution and inclusion body formation *in vivo*

All animal experimental protocols were approved by the Laboratory Animal Research Center of Ajou University Medical Center (approval no. 2020-0033) and complied with the institutional ethical use protocols (NIH Guide for Care and Use of Laboratory Animals). Male ICR mice (8 weeks old, Orientbio,

Seongnam, Korea) were maintained under 12-h light/dark cycles with free access to food and water. Four mice per group were used in this study. The biodistribution and toxicological effects of the MNPs@$SiO_2$(RITC) at 25, 50, and 100 mg/kg were previously reported [5]. The study showed the broad-range tissue distribution of the MNPs@$SiO_2$(RITC) and the brain localization of the MNPs@$SiO_2$(RITC) without blood–brain barrier disruption. The particles did not induce significant toxicological symptoms in terms of growth, behaviors, biochemical changes in serum, and histopathology, even at 100 mg/kg. However, based on our *in vitro* findings, we postulated that there would be subtle toxicity in the brain at 100 mg/kg, which was the maximum concentration evaluated in the previous study. Thus, MNPs@$SiO_2$(RITC) were injected intraperitoneally with sterile saline at 100 mg/kg per mouse. Control mice were injected with sterile saline only. The endpoint was determined at 5 days, based on a previous biodistribution study [5]. Five days after the injection, the mice were anaesthetized with urethane (1.2–1.5 g/kg, intraperitoneally). The hearts were rapidly exposed, and the mice were transcardially perfused with paraformaldehyde (PFA, Sigma-Aldrich, MO, USA). The brains of the PFA-perfused mice were removed and placed in PFA for 24 h. The brains were cryoprotected by immersion in 30% sucrose and then sectioned at 5 μm and stored at −80 °C until analysis.

Frozen sections were incubated in blocking solution containing 1% bovine serum albumin (Sigma-Aldrich, MO, USA) and 10% donkey serum (Sigma-Aldrich, MO, USA) in PBS at RT for 2 h. The sections were stained with anti-d-serine rabbit polyclonal antibody (1:200, Abcam, Cambridge, UK), anti-Iba1 goat polyclonal antibody (1:100, Novus Biologicals, CO, USA), and anti-ubiquitin rabbit polyclonal antibody (1:200, Santa Cruz, CA, USA) diluted in 1% donkey serum in PBS with 0.4% Triton X-100 at 4°C overnight. The sections were rinsed and washed (three times for 10 min) in PBS with 0.4% Triton X-100 and incubated with Alexa Fluor 488- or 647-conjugated secondary donkey antibodies (Invitrogen, CA, USA) at 1:100 dilution in 1% donkey serum in PBS with 0.4% Triton X-100 at RT for 2 h. After the wash steps, the sections were mounted with Vectashield mounting medium containing DAPI (Vector Laboratories, CA, USA), and coverslips were applied. Immunostained sections were scanned using a slide scanner (Axio Scan Z1, Carl Zeiss Microscopy GmbH, Jena, Germany), and regions of interest were viewed under a 40× objective lens on an A1R HD25 confocal microscope (Nikon, Tokyo, Japan) at the 3D immune system imaging core facility of Ajou University. Three-dimensional reconstructions of branch structures were acquired and quantified for number and length, using Imaris 9.2 software (Bitplane, Zurich, Switzerland).

### Statistical analysis

Data were analyzed by analysis of variance (ANOVA) with Bonferroni's multiple-comparison tests, using IBM-SPSS software (IBM, NY, USA). Differences were considered significant at $p < 0.05$.

# Results

### Phenotype changes and NP uptake efficiency of MNPs@$SiO_2$(RITC)-treated microglia

To evaluate the effect of MNPs@$SiO_2$(RITC) on microglia, we first analyzed morphological changes in MNPs@$SiO_2$(RITC)-treated BV2 immortalized murine microglial cells and primary rat microglia. The cells were treated for 12 h with 0.01 or 0.1 μg/μl MNPs@$SiO_2$(RITC) (Fig. 1a) or with 0 (non-treated control), 0.01, or 0.1 ng/μl of LPS as a positive control for morphological activation. Morphological activation (i.e., swollen and round cells) was observed in MNPs@$SiO_2$(RITC)- and LPS-treated microglia (Supplementary Fig. 4). Compared to non-treated control cells, BV2 cells and primary rat microglia showed dose-dependent morphological changes following MNPs@$SiO_2$(RITC) or LPS treatment, but there was no significant difference in cell density.

Iba1 is a microglial marker whose expression is elevated upon microglial activation [28]. MNPs@$SiO_2$(RITC)-treated BV2 cells were stained for Iba1 after 0.01 or 0.1 μg/μl MNPs@$SiO_2$(RITC) treatment for 12 h (Fig. 1b). Iba1-staining fluorescence was increased in a MNPs@$SiO_2$(RITC) dose-dependent manner. Thus, MNPs@$SiO_2$(RITC) treatment induces morphological and biological microglial activation in microglia.

To evaluate detailed changes at the organelle level, the MNPs@$SiO_2$(RITC)-treated BV2 cell ultrastructure was visualized using TEM. MNPs@$SiO_2$(RITC) were clearly visible as black dots throughout the cytoplasm, and the mitochondria showed the most pronounced changes in size and number among the organelles (Fig. 1c). MNPs@$SiO_2$(RITC) were not distributed in the nucleus. The lysosomes, containing MNPs@$SiO_2$(RITC), were approximately 800 nm in diameter. The number of granular structures was increased by ~3-fold in MNPs@$SiO_2$(RITC)-treated BV2 cells compared to 0.01 μg/μl MNPs@$SiO_2$(RITC)-treated and control cells.

In a previous study, the MNPs@$SiO_2$(RITC)-uptake efficiency of MCF-7 mammary gland adenocarcinoma cells was determined using ICP-atomic emission spectroscopy [16]. The efficiency was approximately $10^5$ particles/cell at 2.0 μg/μl MNPs@$SiO_2$(RITC). In this study, BV2 cells were treated with 0.01 or 0.1 μg/μl MNPs@$SiO_2$(RITC), and the uptake efficiency was determined by ICP-MS (Fig. 1d, e). The efficiency was approximately $2.3 \times 10^4$ particles/cell at 0.01 μg/μl MNPs@$SiO_2$(RITC) and $2.0 \times 10^5$ particles/cell at 0.1 μg/μl MNPs@$SiO_2$(RITC). Thus, the MNPs@$SiO_2$(RITC)-uptake efficiency of BV2 cells was approximately 40-fold higher than that of MCF7 cells.

### Transcriptome analysis of MNPs@$SiO_2$(RITC)-treated BV2 cells

To evaluate the biological changes in MNPs@$SiO_2$(RITC)-treated BV2 cells, transcriptome changes after treatment with 0.01 or 0.1 μg/μl MNPs@$SiO_2$(RITC) were investigated using RNA-seq. Changes in gene expression were more pronounced at 0.1 μg/μl than at 0.01 μg/μl. DEGs in 0.1 μg/μl MNPs@$SiO_2$(RITC)- vs. 0.01 μg/μl MNPs@$SiO_2$(RITC)-treated cells were subjected to GO analysis (Fig. 2a); 29 DEGs (51.5% of the total DEGs) were engaged in metabolism, and 18 DEGs (23.9%) were related to signal transduction, especially inflammation (Fig. 2b). A gene co-expression network based on the RNA-seq data was

constructed using IPA. The genes in the network are presented in relation to their function in metabolism and inflammation (Fig. 2c, Supplementary Table 3, and Supplementary Fig. 5). The expression levels of the genes in the network were quantified using RT-qPCR (Fig. 2d). In particular, the expression of chemokine (C-C motif) receptor 1 (*Ccr1*), colony-stimulating factor 3 (*Csf3*), and chemokine (C-X-C motif) ligand 3 (*Cxcl3*) was significantly upregulated and that of formyl peptide receptor 1 (*Fpr1*) and serine (or cysteine) peptidase inhibitor, clade F, member 1 (*Serpinf1*) was significantly downregulated in 0.1 μg/μl MNPs@$SiO_2$(RITC)-treated cells compared to non-treated control cells.

## Disturbances in intracellular amino acids in MNPs@$SiO_2$(RITC)-treated microglia

We profiled 19 cellular amino acids in 0.01 or 0.1 μg/μl MNPs@$SiO_2$(RITC)-treated BV2 cells by ethoxycarbonyl (EOC)/*tert*-butyldimethylsilyl (TBDMS) derivatization and GC-MS (Supplementary Table 4). A star plot revealed increased levels of 7 of the 19 amino acids, including serine, threonine, cysteine, aspartic acid, asparagine, glutamine, and lysine (Fig. 3a). Representative SIM chromatograms showing the changes in the amounts of these seven amino acids in control, 0.01 μg/μl MNPs@$SiO_2$(RITC)-treated, and 0.1 μg/μl MNPs@$SiO_2$(RITC)-treated cells are shown in Fig. 3b, i–iii.

Amino acid profiles and a gene co-expression network were constructed using IPA. The network revealed that changes in the expression of genes related to transport function were highly associated with changes in serine family amino acids, including glycine, cysteine, and serine, in 0.1 and 0.01 μg/μl MNPs@$SiO_2$(RITC)-treated cells compared to non-treated cells (Fig. 3c, Supplementary Table 5, and Supplementary Fig. 6). The expression levels of aryl-hydrocarbon receptor (*Ahr*), cystathionine beta-synthase (*Cbs/Cbsl*), and 130-kDa myosin light chain kinase (*Mylk*) were significantly increased, whereas those of solute carrier family 1 (glutamate/neutral amino acid transporter), member 4 (*Slc1a4*) and solute carrier family 6 (neurotransmitter transporter, glycine), and member 9 (*Slc6a9*) were significantly decreased in 0.1 μg/μl MNPs@$SiO_2$(RITC)-treated cells compared to control cells as indicated by RT-qPCR (Fig. 3d).

## d-Serine secretion in MNPs@$SiO_2$(RITC)-treated microglia *in vitro*

To validate the above findings, we analyzed the extracellular secretion of the above 19 amino acids, including serine family amino acids, in the medium of MNPs@$SiO_2$(RITC)-treated BV2 cells using EOC/TBDMS derivatization and GC-MS (Supplementary Table 6). The increase in serine in the medium was significantly higher than the increases in glycine and cysteine. The representative SIM chromatograms corroborated that serine was more strongly increased in the medium than other serine family amino acids (Fig. 4a). The peak area ratios of serine to the internal standard were approximately 0.10 (control; Fig. 4a, i), 0.12 (0.01 μg/μl treatment; Fig. 4a, ii), and 0.16 (0.1 μg/μl treatment; Fig. 4a, iii).

The GC-MS platform used in this study could not distinguish enantiomers of serine; therefore, we measured d-serine in the media of MNPs@$SiO_2$(RITC)-treated BV2 cells and primary rat microglia using a d-serine-specific enzyme-based method. d-Serine secretion was increased after LPS and

MNPs@$SiO_2$(RITC) treatment in BV2 cells and primary microglia (Fig. 4b). Specifically, the increase in d-serine secretion was the most pronounced in 0.1 μg/μl MNPs@$SiO_2$(RITC)-treated primary microglia. We reanalyzed d-serine by LC-MS using an enantio-separation column. l- and d-Serine were clearly separated, and the extracellular levels of d-serine were increased in 0.1 ng/μl LPS- and 0.1 μg/μl MNPs@$SiO_2$(RITC)-treated primary rat microglia (Fig. 4c, d). l-Serine levels were rather decreased in LPS- and MNPs@$SiO_2$(RITC)-treated cells compared to those in control cells (Fig. 4e).

### ATP and proteasome activity are reduced in neuronal cells cocultured with microglia

To evaluate the effect of activated microglia and secreted d-serine on neuronal cells, we used a Transwell coculture system (Fig. 5a). Microglia, activated with 0.01 or 0.1 μg/μl MNPs@$SiO_2$(RITC) or 0.01 or 0.1 ng/μl LPS for 12 h, were cocultured with SH-SY5Y, cortical, and dopaminergic (DAergic) neurons. After 12 h, the morphology and density of the neuronal cells were observed by microscopy, and cell viability was analyzed (Supplementary Fig. 7). The viability of cortical neurons was decreased, and aggresome-like structures were detected after coculture with 0.1 μg/μl MNPs@$SiO_2$(RITC)-activated microglia. However, cell viability and density were not affected in MNPs@$SiO_2$(RITC)-activated microglia-cocultured SH-SY5Y cells and DAergic neurons.

To evaluate the effect of d-serine secreted from the activated microglia on neuronal cells, we first focused on the mitochondria, because calcium ions from the excitotoxic cascade mainly impair calcium channel-containing organelles such as the mitochondria and the endoplasmic reticulum [29], and the apoptosis cascade is highly associated with the mitochondria [30]. The mitochondrial membrane potential ($\Delta\psi_m$) was analyzed in neuronal cells cocultured with MNPs@$SiO_2$(RITC)-activated microglia (Supplementary Fig. 8). Populations with disrupted $\Delta\psi_m$ were increased in the neuronal cells cocultured with 0.1 μg/μl MNPs@$SiO_2$(RITC)-activated microglia, and the most pronounced decrements (~30%) were observed in cortical neuronal cells. The decrease in $\Delta\psi_m$ was alleviated in the presence of an antagonist of the d-serine binding site of the NMDA receptor, 5,7-dichlorokynurenic acid (DCKA).

Decreases in $\Delta\psi_m$ are highly correlated with decreases in mitochondrial function, specifically ATP production [31]. Intracellular ATP was measured in neuronal cells cocultured with MNPs@$SiO_2$(RITC)-activated microglia. Intracellular ATP levels were reduced in neuronal cells cocultured with 0.1 μg/μl MNPs@$SiO_2$(RITC)-activated microglia, and the most pronounced decrease was observed in cortical neuronal cells (Fig. 5b). The decrease in ATP was also alleviated in the presence of DCKA.

Proteasome activity is highly dependent on the intracellular ATP level [32-34]. Thus, we also analyzed the proteasome activity of neuronal cells cocultured with MNPs@$SiO_2$(RITC)-activated microglia (Fig. 5c). In line with the decrease in intracellular ATP (Fig. 5d-f), proteasome activities were decreased in neuronal cells cocultured with 0.1 μg/μl MNPs@$SiO_2$(RITC)-activated microglia and the decrements were also alleviated in the presence of DCKA (Fig. 5g-i). The impairments of mitochondria and proteasome activity

in the neuronal cells were highly correlated with exposure to d-serine secreted from the MNPs@$SiO_2$(RITC)-activated microglia.

### Inclusion body formation in neuronal cells cocultured with microglia

We assessed the accumulation of ubiquitinated proteins following the reduction in proteasome activity. Ubiquitinated protein levels were significantly higher in neuronal cells cocultured with MNPs@$SiO_2$(RITC)-activated microglia (Fig. 6a). When neuronal cells were cocultured with the 0.1 μg/μl MNPs@$SiO_2$(RITC)-activated microglia, the increase in ubiquitinated proteins was the most pronounced in the cortical neurons. DCKA suppressed the increases in ubiquitinated proteins.

Immunocytochemical analysis revealed a dramatic increase in inclusion bodies in cortical neuronal cells cocultured with 0.1 μg/μl MNPs@$SiO_2$(RITC)-activated microglia (Fig. 6b). However, inclusion body formation was not detected in SH-SY5Y cells (data not shown). We observed a dose-dependent increase in inclusion bodies in the dopaminergic neuronal cells cocultured with MNPs@$SiO_2$(RITC)-activated microglia (Supplementary Fig. 9), but not as strong as that observed in the cortical neuronal cells (Fig. 6c).

### Microglial activation and d-serine secretion in MNPs@$SiO_2$(RITC)-treated microglia *in vivo*

To assess MNPs@$SiO_2$(RITC) nanotoxicity on microglia *in vivo*, mice were intraperitoneally injected with MNPs@$SiO_2$(RITC) for 5 days. Mouse brains were collected and divided into cortex and striatum for immunohistochemical analysis (Fig. 7a, b). MNPs@$SiO_2$(RITC) were homogeneously distributed in the brain and preferentially accumulated in Iba1-positive microglia. Moreover, MNPs@$SiO_2$(RITC)- and Iba1-positive microglia showed an activated morphology. d-Serine was distributed around the activated microglia. A 3D reconstruction of microglia morphology clearly showed that the branched structures of microglia were significantly shortened in MNPs@$SiO_2$(RITC)-treated mice (Fig. 7c). Cell numbers were not affected (Fig. 7d), but ubiquitin aggresome-like cell structures were detected in brain sections of MNPs@$SiO_2$(RITC)-treated mice (Supplementary Fig. 10).

## Discussion

The present study combined conventional biomolecular and integrated omics-based analyses to evaluate the MNPs@$SiO_2$(RITC)-induced activation of microglia and the neuronal toxicity of the activated microglia. Especially, we profiled the transcriptome and amino acids in the MNPs@$SiO_2$(RITC)-treated microglia and subjected significantly changed factors to functional analysis to deduce relationships between microglial activation and d-serine-related mechanisms after NP exposure. We demonstrated that high-concentration MNPs@$SiO_2$(RITC) induced microglial activation and d-serine secretion. The high concentration of d-serine secreted from the activated microglia induced neuronal cell death, especially in cortical neurons, via excitotoxicity, including mitochondrial depolarization, a reduction in intracellular ATP, a decrease in proteasomal activity, and the accumulation of ubiquitinated proteins. Our results indicate

that minimizing NP usage or exposure is important for preventing nanotoxicity related to microglial activation and concomitant excitotoxicity to neurons in the brain.

We observed intracellular granular structure formation and increment of d-Serine secretion in MNPs@$SiO_2$(RITC)-treated microglia. d-Serine secretion in microglia responds to amyloid beta, LPS, and secreted amyloid precursor protein [35, 36], but d-serine secretion in NP-treated microglia had not been reported. Concomitant with the increase in d-serine secretion, gene expression related to the transport of serine family amino acids was increased as indicated by combined transcriptome and amino acid profiling analyses. In astrocytes, d-serine secretion mechanisms include synaptosomal-associated proteins receptor (SNARE)-dependent exocytosis as well as non-exocytic mechanisms such as volume-regulated anion channel, alanine–serine–cysteine transporter, and gap junction hemichannels. The mechanism of d-serine release by microglia is still unclear [36, 37]. Moreover, although we have previously observed excitotoxic glutamate production in MNPs@$SiO_2$(RITC)-treated HEK293 cells based on metabotranscriptome analysis [26], the mechanisms of d-serine production and secretion in MNPs@$SiO_2$(RITC)-treated microglia have not been unraveled. In MNPs@$SiO_2$(RITC)-treated microglia, d-serine did not colocalize with VAMP2 nor NPY, which are exocytic vesicle markers in astrocytes (Supplementary Fig. 11) [38, 39], suggesting that microglia utilize a pathway for d-serine secretion different from that of astrocytes and detailed future analysis is required to reveal the specific mechanism.

The MNPs@$SiO_2$(RITC)-induced d-serine secretion reduced the intracellular ATP level, mitochondrial function, and proteasomal activity in neuronal cells via excitotoxicity. Excitotoxicity is highly correlated with the pathological phenotype of neurodegenerative disease [40, 41], and it is triggered by the opening of calcium channels, including the NMDA receptor, by agonists. Physiologically, extracellular and intracellular calcium ion concentrations differ by 20,000-fold (mM vs. 100 nM) [42]. Massive calcium ion influx induces a calcium ion imbalance, mainly in the mitochondria and endoplasmic reticulum [43]. Owing to this imbalance, mitochondrial dysfunction occurs and ATP production decreases [29, 44]. ATP is essential for ubiquitination, de-ubiquitination, and proteasome complex assembly [32–34]. When ATP strongly decreases, the ubiquitin-proteasome system is corrupted, resulting in the aggregation and accumulation of defective proteins in cells. In neurons, such protein aggregations are histopathological biomarkers for neurodegenerative diseases [45]. Thus, the d-serine level in the brain may be monitored after NP exposure as a secondary (indirect) phenotype of neuronanotoxicity.

Cortical neuronal cells reacted more sensitively to d-serine-induced excitotoxicity than dopaminergic neurons. Overactivation of the NMDA receptor by d-serine induces neuronal death and protein aggregation [46, 47]. In this study, cortical Lewy bodies, a pathological feature of Alzheimer's disease [48], were detected in *in vitro* MNPs@$SiO_2$(RITC)-activated microglia-cocultured cortical neurons and in the mouse brain *in vivo*. Neuronal cells in the MNPs@$SiO_2$(RITC)-activated microglia coculture system showed decreased viability, along with decreases in intracellular ATP and proteasome activity, and the effects were the most pronounced in cortical neurons. Our previous study showed that dopaminergic neurons are more vulnerable to MNPs@$SiO_2$(RITC)-induced nanotoxicity (direct effect) than cortical

neuronal cells [8]. In this study, cortical neurons responded more sensitively to d-serine secreted from MNPs@$SiO_2$(RITC)-activated microglia than DAergic neurons. This is consistent with the finding that cortical neurons are more vulnerable to excitotoxic conditions than DAergic neurons, because endogenous dopamine from DAergic neurons can block excitotoxicity-induced calcium signals and plays a major role in conserving calcium homeostasis in cells [49]. Moreover, molecules abundant in DAergic neurons, including kynurenic acid, brain-derived neurotrophic factor, and prostaglandin A1, protect against excitotoxicity in DAergic neurons [50–52]. Collectively, we showed the induction of a series of dysfunctions in neuronal cells by d-serine secreted from MNPs@$SiO_2$(RITC)-activated microglia, suggesting the secondary toxicity of NPs.

# Conclusions

Based on transcriptomics and amino acid profiling, this study revealed that NP-induced microglial activation is associated with excitotoxic d-serine secretion. The present findings suggest that exposure to NPs can directly activate microglia and indirectly be deleterious to neurons. These results highlight the importance of the safety evaluation of NPs and the assessment of secondary nanotoxicity effects.

# Abbreviations

Ahr: aryl-hydrocarbon receptor; ANOVA: analysis of variance; BBB: blood–brain barrier; *Cbs/Cbsl*: cystathionine beta-synthase; CCCP: carbonyl cyanide m-chlorophenyl hydrazine; *Ccr1*: chemokine (C-C motif) receptor 1; CNS: central nervous system; $CoFe_2O_3$: cobalt ferrite; *Csf3*: colony-stimulating factor 3; *Cxcl3*: chemokine (C-X-C motif) ligand 3; DCKA: 5,7-dichlorokynurenic acid; DEG: differentially expressed gene; DsdSC: $_D$-serine dehydratase from *Saccharomyces cerevisiae*; EOC: ethoxycarbonyl; FACS: fluorescence-activated cell sorting; *Fpr1*: formyl peptide receptor 1; GC: gas chromatography; GO: gene ontology; HF: hydrogen fluoride; ICP-MS: inductively coupled plasma mass spectrometry; IPA: ingenuity pathway analysis; JC-1: 5,5',6,6'-tetrachloro-1,1',3,3'- tetraethylbenzimidazolyl carbocyanine iodide; LC: liquid chromatography; LDH: lactate dehydrogenase; MGI: mouse genome informatics; MNPs: Magnetic nanoparticles; *Mylk*: 130-kDa myosin light chain kinase; NADH: nicotinamide adenine dinucleotide; NeuN: neuronal nuclei; NMDA: *N*-methyl-$_D$-aspartate; NO: nitric oxide; NPs: nanoparticles; NPY: neuropeptide Y; PFA: paraformaldehyde; RITC: rhodamine B isothiocyanate; ROS: reactive oxygen species; RT: room temperature; RT-qPCR: quantitative reverse transcription PCR; *Serpinf1*: serine (or cysteine) peptidase inhibitor, clade F, member 1; SIM: selected-ion monitoring; *Slc1a4*: solute carrier family 1 (glutamate/neutral amino acid transporter), member 4; *Slc6a9*: solute carrier family 6 (neurotransmitter transporter, glycine), and member 9; SNARE: synaptosomal-associated proteins receptor; TBDMS: tert-butyldimethylsilyl; TEM: transmission electron microscopy; TH: tyrosine hydrolase; VAMP2: vesicle-associated membrane protein 2; XRD: X-ray diffraction

# Declarations

## Ethical Approval and Consent to participate

All animal experimental protocols were approved by the Laboratory Animal Research Center of Ajou University Medical Center (approval no. 2020-0033) and complied with the institutional ethical use protocols (NIH Guide for Care and Use of Laboratory Animals).

## Consent for publication

Not applicable.

## Availability of data and materials

The data supporting the findings of this study are available from the corresponding author, upon reasonable request. Transcriptome sequencing and quantification data are available in the GEO database under the following accession number: GSE154250.

## Availability of supporting data

The online version contains supplementary material available at https://doi.org/10.1186/s#######.

## Competing interests

The authors declare that they have no competing interests.


## Funding

This work was supported by grants from the National Research Foundation (NRF), funded by the Ministry of Science and ICT (MSIT) in Korea [2020R1C1C1008366, 2020R1A4A4079722, 2020M3E5D9080661, and 2016M3C7A1904392].


## Authors' contributions

T.H.S., D.Y.L., and G.L. contributed to the conception and design of the project. T.H.S., D.Y.L., and G.L. analyzed the data and wrote the manuscript. T.H.S., D.Y.L., B.M., S.B., Y.C.N., C.Y., and H.S.L. performed experiments. B.M., S.B., Y.C.N., C.Y., H.S.L., and M.J.P. provided reagents and help with data interpretation. All authors read and approved the final manuscript.


## Acknowledgements

The authors thank Ji Eun Lee, Sinae Ahn, Sun Young Che, and the Ajou Core-Facility Center for technical assistance and cell imaging analysis.


## Authors information

Tae Hwan Shin and Da Yeon Lee contributed equally to this work.

**Affiliations**

**Department of Physiology, Ajou University School of Medicine, Suwon, Republic of Korea**

Tae Hwan Shin, Da Yeon Lee, Balachandran Manavalan, Shaherin Basith & Gwang Lee

**Western Seoul Center, Korea Basic Science Institute, Seoul, Republic of Korea**

Yun-Cheol Na

**Seoul Center, Korea Basic Science Institute, Seoul, Republic of Korea**

Cheolho Yoon

**College of Pharmacy, Sunchon National University, Suncheon, Republic of Korea**

Hyeon-Seong Lee & Man Jeong Paik

**Department of Molecular Science and Technology, Ajou University, Suwon, Republic of Korea**

Gwang Lee

# References

1. Zhou Y, Peng Z, Seven ES, Leblanc RM. Crossing the blood-brain barrier with nanoparticles. J Control Release. 2018;270:290–303.
2. Cheng Y, Dai Q, Morshed RA, Fan X, Wegscheid ML, Wainwright DA, Han Y, Zhang L, Auffinger B, Tobias AL, et al. Blood-brain barrier permeable gold nanoparticles: an efficient delivery platform for enhanced malignant glioma therapy and imaging. Small. 2014;10:5137–50.
3. Liang H, Chen A, Lai X, Liu J, Wu J, Kang Y, Wang X, Shao L. Neuroinflammation is induced by tongue-instilled ZnO nanoparticles via the Ca(2+)-dependent NF-kappaB and MAPK pathways. Part Fibre Toxicol. 2018;15:39.
4. Xu G, Mahajan S, Roy I, Yong KT. Theranostic quantum dots for crossing blood-brain barrier in vitro and providing therapy of HIV-associated encephalopathy. Front Pharmacol. 2013;4:140.
5. Kim JS, Yoon TJ, Yu KN, Kim BG, Park SJ, Kim HW, Lee KH, Park SB, Lee JK, Cho MH. Toxicity and tissue distribution of magnetic nanoparticles in mice. Toxicol Sci. 2006;89:338–47.
6. Mushtaq G, Khan JA, Joseph E, Kamal MA. Nanoparticles, Neurotoxicity and Neurodegenerative Diseases. Curr Drug Metab. 2015;16:676–84.
7. Linse S, Cabaleiro-Lago C, Xue WF, Lynch I, Lindman S, Thulin E, Radford SE, Dawson KA. Nucleation of protein fibrillation by nanoparticles. Proc Natl Acad Sci U S A. 2007;104:8691–6.
8. Phukan G, Shin TH, Shim JS, Paik MJ, Lee JK, Choi S, Kim YM, Kang SH, Kim HS, Kang Y, et al. Silica-coated magnetic nanoparticles impair proteasome activity and increase the formation of

cytoplasmic inclusion bodies in vitro. Sci Rep. 2016;6:29095.

9. Amor S, Peferoen LA, Vogel DY, Breur M, van der Valk P, Baker D, van Noort JM. Inflammation in neurodegenerative diseases–an update. Immunology. 2014;142:151–66.
10. Ambrose N, Rodriguez M, Waters KA, Machaalani R.. Brain, Behavior. Microglia in the human infant brain and factors that affect expression. & Immunity - Health. 2020;7:100117. https://doi.org/10.1016/j.bbih.2020.100117.
11. Hutter E, Boridy S, Labrecque S, Lalancette-Hebert M, Kriz J, Winnik FM, Maysinger D. Microglial response to gold nanoparticles. ACS Nano. 2010;4:2595–606.
12. Lee A, Arachchige BJ, Henderson R, Pow D, Reed S, Aylward J, McCombe PA. Elevated plasma levels of D-serine in some patients with amyotrophic lateral sclerosis. Amyotroph Lateral Scler Frontotemporal Degener. 2020:1–5.
13. Zhang JB, Chang S, Xu P, Miao M, Wu H, Zhang Y, Zhang T, Wang H, Zhang J, Xie C, et al. Structural Basis of the Proton Sensitivity of Human GluN1-GluN2A NMDA Receptors. Cell Rep. 2018;25:3582–90.
14. Shin TH, Lee DY, Lee HS, Park HJ, Jin MS, Paik MJ, Manavalan B, Mo JS, Lee G. Integration of metabolomics and transcriptomics in nanotoxicity studies. BMB Rep. 2018;51:14–20.
15. Delogu F, Kunath BJ, Evans PN, Arntzen M, Hvidsten TR, Pope PB. Integration of absolute multi-omics reveals dynamic protein-to-RNA ratios and metabolic interplay within mixed-domain microbiomes. Nat Commun. 2020;11:4708.
16. Yoon TJ, Kim JS, Kim BG, Yu KN, Cho MH, Lee JK. Multifunctional nanoparticles possessing a "magnetic motor effect" for drug or gene delivery. Angew Chem Int Ed Engl. 2005;44:1068–71.
17. Beck GR Jr, Ha SW, Camalier CE, Yamaguchi M, Li Y, Lee JK, Weitzmann MN. Bioactive silica-based nanoparticles stimulate bone-forming osteoblasts, suppress bone-resorbing osteoclasts, and enhance bone mineral density in vivo. Nanomedicine. 2012;8:793–803.
18. Shin TH, Lee DY, Lee HS, Park HJ, Jin MS, Paik MJ, Manavalan B, Mo JS, Lee G. Integration of metabolomics and transcriptomics in nanotoxicity studies. BMB Rep. 2018.
19. Shin TH, Ketebo AA, Lee DY, Lee S, Kang SH, Basith S, Manavalan B, Kwon DH, Park S, Lee G. Decrease in membrane fluidity and traction force induced by silica-coated magnetic nanoparticles. J Nanobiotechnology. 2021;19:21.
20. Shin TH, Lee DY, Ketebo AA, Lee S, Manavalan B, Basith S, Ahn C, Kang SH, Park S, Lee G. Silica-Coated Magnetic Nanoparticles Decrease Human Bone Marrow-Derived Mesenchymal Stem Cell Migratory Activity by Reducing Membrane Fluidity and Impairing Focal Adhesion. Nanomaterials (Basel). 2019, 9:1475.
21. Shin TH, Seo C, Lee DY, Ji M, Manavalan B, Basith S, Chakkarapani SK, Kang SH, Lee G, Paik MJ, Park CB. Silica-coated magnetic nanoparticles induce glucose metabolic dysfunction in vitro via the generation of reactive oxygen species. Arch Toxicol. 2019;93:1201–12.
22. Ketebo AA, Shin TH, Jun M, Lee G, Park S. Effect of silica-coated magnetic nanoparticles on rigidity sensing of human embryonic kidney cells. J Nanobiotechnology. 2020;18:170.

23. Wang AL, Yu AC, Lau LT, Lee C, Wu le M, Zhu X, Tso MO. Minocycline inhibits LPS-induced retinal microglia activation. Neurochem Int. 2005;47:152–8.
24. Trapnell C, Roberts A, Goff L, Pertea G, Kim D, Kelley DR, Pimentel H, Salzberg SL, Rinn JL, Pachter L. Differential gene and transcript expression analysis of RNA-seq experiments with TopHat and Cufflinks. Nat Protoc. 2012;7:562–78.
25. Eppig JT, Richardson JE, Kadin JA, Ringwald M, Blake JA, Bult CJ. Mouse Genome Informatics (MGI): reflecting on 25 years. Mamm Genome. 2015;26:272–84.
26. Shim W, Paik MJ, Nguyen DT, Lee JK, Lee Y, Kim JH, Shin EH, Kang JS, Jung HS, Choi S, et al. Analysis of changes in gene expression and metabolic profiles induced by silica-coated magnetic nanoparticles. ACS Nano. 2012;6:7665–80.
27. Kim YJ, Park HJ, Lee G, Bang OY, Ahn YH, Joe E, Kim HO, Lee PH. Neuroprotective effects of human mesenchymal stem cells on dopaminergic neurons through anti-inflammatory action. Glia. 2009;57:13–23.
28. Hopperton KE, Mohammad D, Trepanier MO, Giuliano V, Bazinet RP. Markers of microglia in post-mortem brain samples from patients with Alzheimer's disease: a systematic review. Mol Psychiatry. 2018;23:177–98.
29. Zundorf G, Reiser G. Calcium dysregulation and homeostasis of neural calcium in the molecular mechanisms of neurodegenerative diseases provide multiple targets for neuroprotection. Antioxid Redox Signal. 2011;14:1275–88.
30. Wang C, Youle RJ. The role of mitochondria in apoptosis*. Annu Rev Genet. 2009;43:95–118.
31. Vojtiskova A, Jesina P, Kalous M, Kaplanova V, Houstek J, Tesarova M, Fornuskova D, Zeman J, Dubot A, Godinot C. Mitochondrial membrane potential and ATP production in primary disorders of ATP synthase. Toxicol Mech Methods. 2004;14:7–11.
32. Shang F, Taylor A. Ubiquitin-proteasome pathway and cellular responses to oxidative stress. Free Radic Biol Med. 2011;51:5–16.
33. Zungu M, Schisler JC, Essop MF, McCudden C, Patterson C, Willis MS. Regulation of AMPK by the ubiquitin proteasome system. Am J Pathol. 2011;178:4–11.
34. Glickman MH, Ciechanover A. The ubiquitin-proteasome proteolytic pathway: destruction for the sake of construction. Physiol Rev. 2002;82:373–428.
35. Martineau M, Baux G, Mothet JP. D-serine signalling in the brain: friend and foe. Trends Neurosci. 2006;29:481–91.
36. Beltran-Castillo S, Eugenin J, von Bernhardi R. Impact of Aging in Microglia-Mediated D-Serine Balance in the CNS. Mediators Inflamm. 2018, 2018:7219732.
37. Henneberger C, Papouin T, Oliet SH, Rusakov DA. Long-term potentiation depends on release of D-serine from astrocytes. Nature. 2010;463:232–6.
38. Mothet JP, Pollegioni L, Ouanounou G, Martineau M, Fossier P, Baux G. Glutamate receptor activation triggers a calcium-dependent and SNARE protein-dependent release of the gliotransmitter D-serine.

Proc Natl Acad Sci U S A. 2005;102:5606–11.
39. Ramamoorthy P, Whim MD. Trafficking and fusion of neuropeptide Y-containing dense-core granules in astrocytes. J Neurosci. 2008;28:13815–27.
40. Van Damme P, Dewil M, Robberecht W, Van Den Bosch L. Excitotoxicity and amyotrophic lateral sclerosis. Neurodegener Dis. 2005;2:147–59.
41. Celsi F, Pizzo P, Brini M, Leo S, Fotino C, Pinton P, Rizzuto R. Mitochondria, calcium and cell death: a deadly triad in neurodegeneration. Biochim Biophys Acta. 2009;1787:335–44.
42. Eyo UB, Gu N, De S, Dong H, Richardson JR, Wu LJ. Modulation of microglial process convergence toward neuronal dendrites by extracellular calcium. J Neurosci. 2015;35:2417–22.
43. Ham J, Lim W, Whang KY, Song G. Butylated hydroxytoluene induces dysregulation of calcium homeostasis and endoplasmic reticulum stress resulting in mouse Leydig cell death. Environ Pollut. 2020;256:113421.
44. Son G, Han J. Roles of mitochondria in neuronal development. BMB Rep. 2018;51:549–56.
45. Vilchez D, Saez I, Dillin A. The role of protein clearance mechanisms in organismal ageing and age-related diseases. Nat Commun. 2014;5:5659.
46. Esposito S, Pristera A, Maresca G, Cavallaro S, Felsani A, Florenzano F, Manni L, Ciotti MT, Pollegioni L, Borsello T, Canu N. Contribution of serine racemase/d-serine pathway to neuronal apoptosis. Aging Cell. 2012;11:588–98.
47. Paul P, de Belleroche J. Experimental approaches for elucidating co-agonist regulation of NMDA receptor in motor neurons: Therapeutic implications for amyotrophic lateral sclerosis (ALS). J Pharm Biomed Anal. 2015;116:2–6.
48. Edison P, Ahmed I, Fan Z, Hinz R, Gelosa G, Ray Chaudhuri K, Walker Z, Turkheimer FE, Brooks DJ. Microglia, amyloid, and glucose metabolism in Parkinson's disease with and without dementia. Neuropsychopharmacology. 2013;38:938–49.
49. Vaarmann A, Kovac S, Holmstrom KM, Gandhi S, Abramov AY. Dopamine protects neurons against glutamate-induced excitotoxicity. Cell Death Dis. 2013;4:e455.
50. Canudas AM, Pezzi S, Canals JM, Pallas M, Alberch J. Endogenous brain-derived neurotrophic factor protects dopaminergic nigral neurons against transneuronal degeneration induced by striatal excitotoxic injury. Brain Res Mol Brain Res. 2005;134:147–54.
51. Miranda AF, Boegman RJ, Beninger RJ, Jhamandas K. Protection against quinolinic acid-mediated excitotoxicity in nigrostriatal dopaminergic neurons by endogenous kynurenic acid. Neuroscience. 1997;78:967–75.
52. Qin ZH, Wang Y, Chen RW, Wang X, Ren M, Chuang DM, Chase TN. Prostaglandin A(1) protects striatal neurons against excitotoxic injury in rat striatum. J Pharmacol Exp Ther. 2001;297:78–87. PMID: 11259530.

# Supplementary Material

**Additional file 1:Supplementary Table 1**. Quantitative real-time PCR primer sequences for genes encoding transcriptomic network related genes

**Additional file 2:Supplementary Table 2**. Quantitative real-time PCR primer sequences for genes encoding combined transcriptome and amino acid profiles network related genes

**Additional file 3:Supplementary Table 3**. Ingenuity Pathway Analysis-based profiles of transcriptome of BV2 cells treated with MNPs@$SiO_2$(RITC)

**Additional file 4:Supplemenatary Table 4.** Amino acid amount in cell mass of MNPs@$SiO_2$(RITC)-treated BV2 cells

**Additional file 5: Supplementary Table 5**. Ingenuity Pathway Analysis-based profiles of transcriptome and amino acids of BV2 cells treated with MNPs@$SiO_2$(RITC)

**Additional file 6: Supplemenatary Table 6.** Concentrations of secreted amino acids in media of MNPs@$SiO_2$(RITC)-treated BV2 cells

**Additional file 7: Supplementary Figure 1.** Transmission electron microscope images for MNPs@$SiO_2$(RITC). Scale bar = 20 nm.

**Additional file 8: Supplementary Figure 2.** XRD spectrum of MNPs@$SiO_2$(RITC). Peaks in $30^o$, $36^o$, $44^o$, $57^o$ and $64^o$ are specific patterns of cobalt ferrite and the broad peak between $20^o$ and $40^o$ indicate the amorphous silica beads.

**Additional file 9: Supplementary Figure 3.** Characterization of primary rat neuronal cells and microglia. **a** Immunofluorescence of cortical neurons stained with anti-NeuN antibody. **b** Immunofluorescence of dopaminergic neurons stained with anti-TH antibody. Scale bar = 10 μm. **c** FACS analysis for OX-42 expression in primary rat microglia. Percentage indicates positively stained population of cells.

**Additional file 10: Supplementary Figure 4.** Microglia activation after MNPs@$SiO_2$(RITC) treatment. Morphological analysis of **a** BV2 and **b** primary rat microglia. Scale bar = 50 μm. Red; MNPs@$SiO_2$(RITC).

**Additional file 11: Supplementary Figure 5.** Transcriptomic network of 0.01 μg/μl treated BV2 cells. Metabolism and inflammation related genes and network of 0.01 μg/μl treated BV2 cells was constructed algorithmically by IPA. Red and green areas indicate up- and downregulated genes, respectively.

**Additional file 12: Supplementary Figure 6.** Combinatorial analysis of RNA-seq and intracellular amino acid profiles 0.01 μg/μl MNPs@$SiO_2$(RITC) treated BV2. Transcriptome combined with amino acids profiles network were constructed algorithmically by IPA in 0.01 μg/μl MNPs@$SiO_2$(RITC) treated BV2. Red and green areas indicate up- and downregulated genes, respectively. Cut off fold change ±1.5 for genes and ±1.2 for amino acids were used.

**Additional file 13: Supplementary Figure 7.** Evaluation of cytotoxicity on neuronal cells in coculture system with activated microglia. **a** Morphological analysis and cell density observation of SH-SY5Y, DAergic (dopaminergic), and cortical neurons. Scale bar = 50 μm. **b** MTS assay for evaluation of cocultured neurons viability. Data were normalized with non-treated control and represent mean ± SD of three independent experiments. *$p < 0.05$ *vs* non-treated control.

**Additional file 14: Supplementary Figure 8.** Evaluation of changes in mitochondria membrane potential in MNPs@$SiO_2$(RITC) treated primary rat microglia cocultured neuronal cells. mitochondria membrane potentials were analyzed using 5,5',6,6'-tetrachloro-1,1',3,3'- tetraethylbenzimidazolyl carbocyanine iodide (JC-1). Red fluorescence (high membrane potential) and green fluorescence (low membrane potential) were measured by fluorescence-activated cell sorting (FACS). Percentage indicates the portion of cells with low mitochondria membrane potential. Carbonyl cyanide *m*-chlorophenyl hydrazine (CCCP) were used as positive control for decreasing mitochondria membrane potential.

**Additional file 15: Supplementary Figure 9.** Inclusion body formation in MNPs@$SiO_2$(RITC) treated microglia cocultured dopaminergic neurons. Images of inclusion body formation were acquired by immunostaining with ubiquitin (green), α-synuclein (red), and nucleus (blue) Scale bar = 10 μm.

**Additional file 16: Supplementary Figure 10.** Inclusion body formation in MNPs@$SiO_2$(RITC) treated mice brains. Images of inclusion body formation were acquired by immunostaining with ubiquitin (green), MNPs@$SiO_2$(RITC) (red), and nucleus (blue). Black scale bar = 100 μm. White scale bar = 10 μm. White arrowhead indicates inclusion body without colocalized to MNPs@$SiO_2$(RITC) and black arrowhead indicates inclusion body with colocalized to MNPs@$SiO_2$(RITC).

**Additional file 17: Supplementary Figure 11.** Immunostaining analysis for exocytic vesicle marker and D-serine in MNPs@$SiO_2$(RITC) treated microglia. Images of exocytic vesicle marker and D-serine were acquired by immunostaining with MNPs@$SiO_2$(RITC) (red), VAMP2 or NPY (green), D-serine (violet), and nucleus (blue). Stained with VAMP2 in **a** BV2 and **b** primary rat microglia and stained with NPY in **c** BV2 and **d** primary rat microglia were analysed. Scale bar = 20 μm.

# Figures

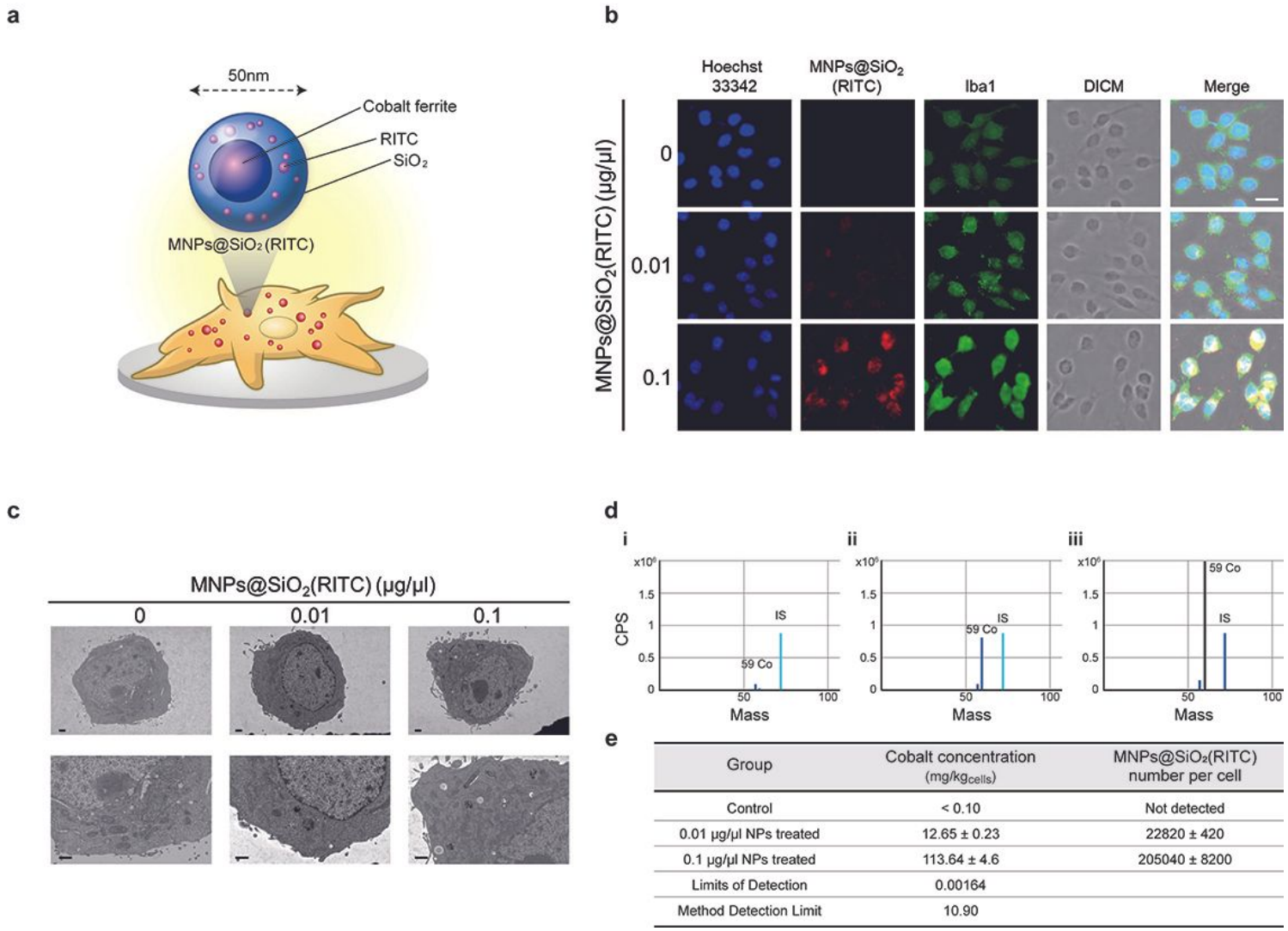


| Group | Cobalt concentration ($mg/kg_{cells}$) | MNPs@SiO₂(RITC) number per cell |
|---|---|---|
| Control | < 0.10 | Not detected |
| 0.01 μg/μl NPs treated | 12.65 ± 0.23 | 22820 ± 420 |
| 0.1 μg/μl NPs treated | 113.64 ± 4.6 | 205040 ± 8200 |
| Limits of Detection | 0.00164 | |
| Method Detection Limit | 10.90 | |

## Figure 1

TEM analysis of MNPs@SiO2(RITC)-treated BV2 cells. a Schematic representation of the MNPs@SiO2(RITC) composition. b Immunostaining image of Iba1 (green), MNPs@SiO2(RITC) (red), and the nucleus (blue). Scale bar = 20 μm. c Representative TEM images of MNPs@SiO2(RITC)-treated BV2 cells. Magnified images are presented in the bottom panels. The red arrow head indicates MNPs@SiO2(RITC) in the cell, and the yellow arrow head indicates a granular structure. Scale bar = 1 μm. d ICP-MS peak of the cobalt ion in the control and MNPs@SiO2(RITC)-treated microglia. IS = internal standard. e Quantification of the cobalt concentration and MNPs@SiO2(RITC) particles in each MNPs@SiO2(RITC)-treated cell.

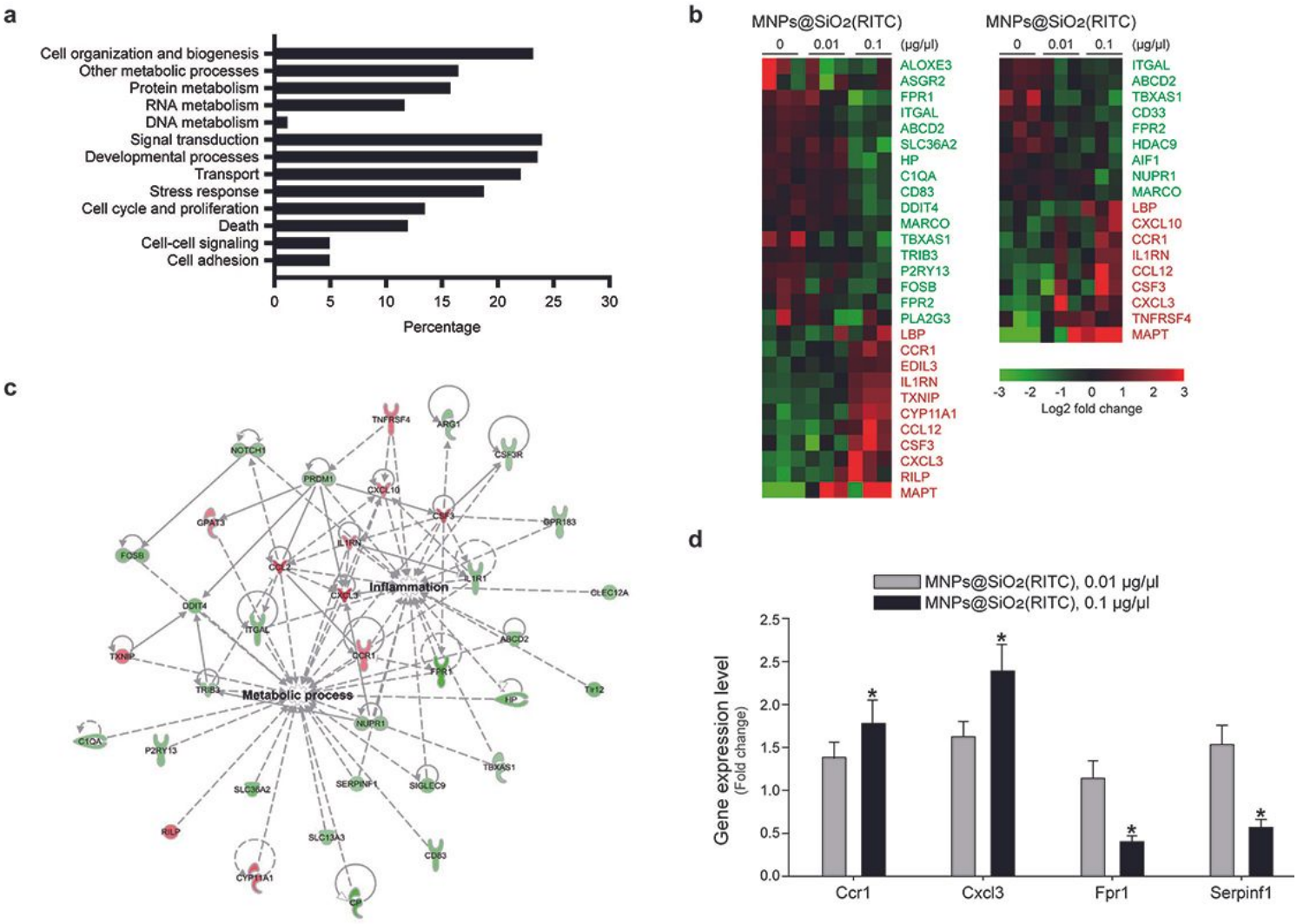


## Figure 2

RNA-seq-based transcriptome analysis of BV2 cells treated with MNPs@SiO2(RITC) for 12 h. a Categorization of DEGs identified by RNA-seq. DEGs were analyzed using the MGI GO tool. Metabolism-related genes are highlighted. b Heat map of DEGs (fold change >1.5 or <−1.5), including 29 DEGs related to metabolism (left panel) and 18 DEGs related to inflammation (right panel), in control cells and 0.1 and 0.01 μg/μl MNPs@SiO2(RITC)-treated cells. c Metabolism- and inflammation-related gene network for 0.1 μg/μl-treated BV2 cells constructed by IPA. The red and green areas indicate the up- and downregulated genes, respectively.

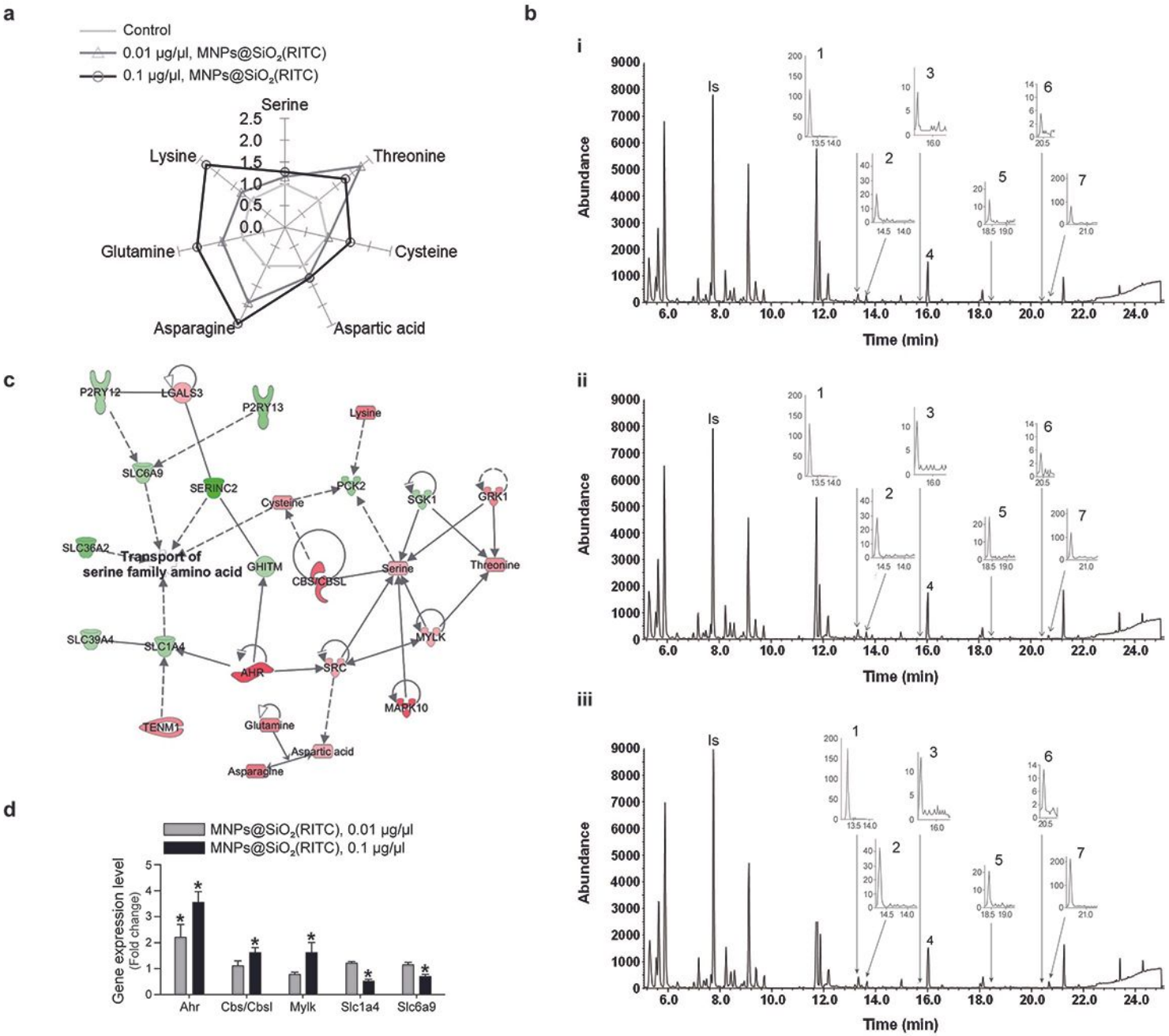


## Figure 3

Combined RNA-seq and intracellular amino acid profiling analyses of BV2 cells treated with MNPs@SiO2(RITC) for 12 h. a Star plot showing altered levels of 7 out of 19 amino acids evaluated in BV2 cells after MNPs@SiO2(RITC) treatment. Target levels were normalized to the corresponding values in the non-treated control group. b SIM chromatograms of the 7 amino acids in (i) control, (ii) 0.01 μg/μl, and (iii) 0.1 μg/μl MNPs@SiO2(RITC)-treated BV2 cells. c Transcriptome and amino acid network for 0.1 μg/μl MNPs@SiO2(RITC)-treated BV2 cells constructed IPA. Red and green areas indicate the up- and downregulated genes, respectively. As cut-offs, fold changes >1.5 or <−1.5 for genes and of >1.2 or <−1.2 for amino acids were used. d RT-qPCR analysis of gene expression in each group, using GAPDH as an

internal control. Data represent the mean ± standard deviation of three independent experiments. *p < 0.05 vs. non-treated control.

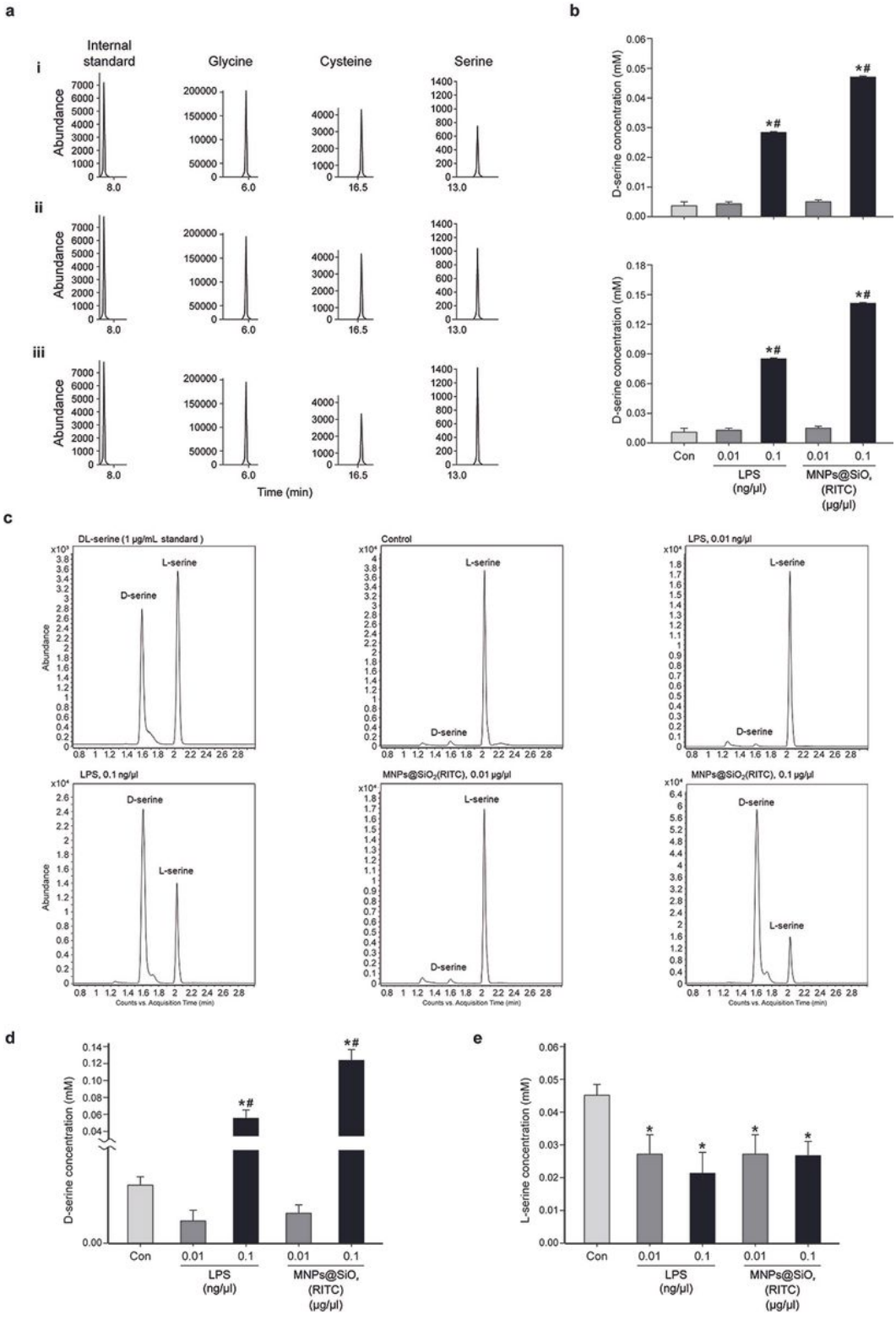


## Figure 4

Analysis of the changes in serine family amino acids and quantification of L-and D-serine secretion by BV2 cells treated with MNPs@SiO2(RITC). a SIM chromatograms of glycine, cysteine, and serine in (i) control (ii) 0.01 μg/μl, and (iii) 0.1 μg/μl MNPs@SiO2(RITC)-treated microglia. The internal standard was

norvaline. b Quantitative analysis of D-serine in the medium of MNPs@SiO2(RITC)-treated microglial cells using an enzyme-based system. Data were normalized to the control and represent the mean ± SD of three independent experiments. *p < 0.05 vs. non-treated control. c Multiple reaction monitoring peaks of L- and D-serine in the control, 0.01 μg/μl, and 0.1 μg/μl MNPs@SiO2(RITC)- and 0.01 and 0.1 ng/μl LPS-treated primary rat microglia. Quantification and statistical analysis of L- d and D-serine e in control, 0.01 μg/μl, and 0.1 μg/μl MNPs@SiO2(RITC)- and 0.01 and 0.1 ng/μl LPS-treated primary rat microglia. *p < 0.05 vs. non-treated control. #p < 0.05 vs. 0.01 μg/μl MNPs@SiO2(RITC)-treated cells.

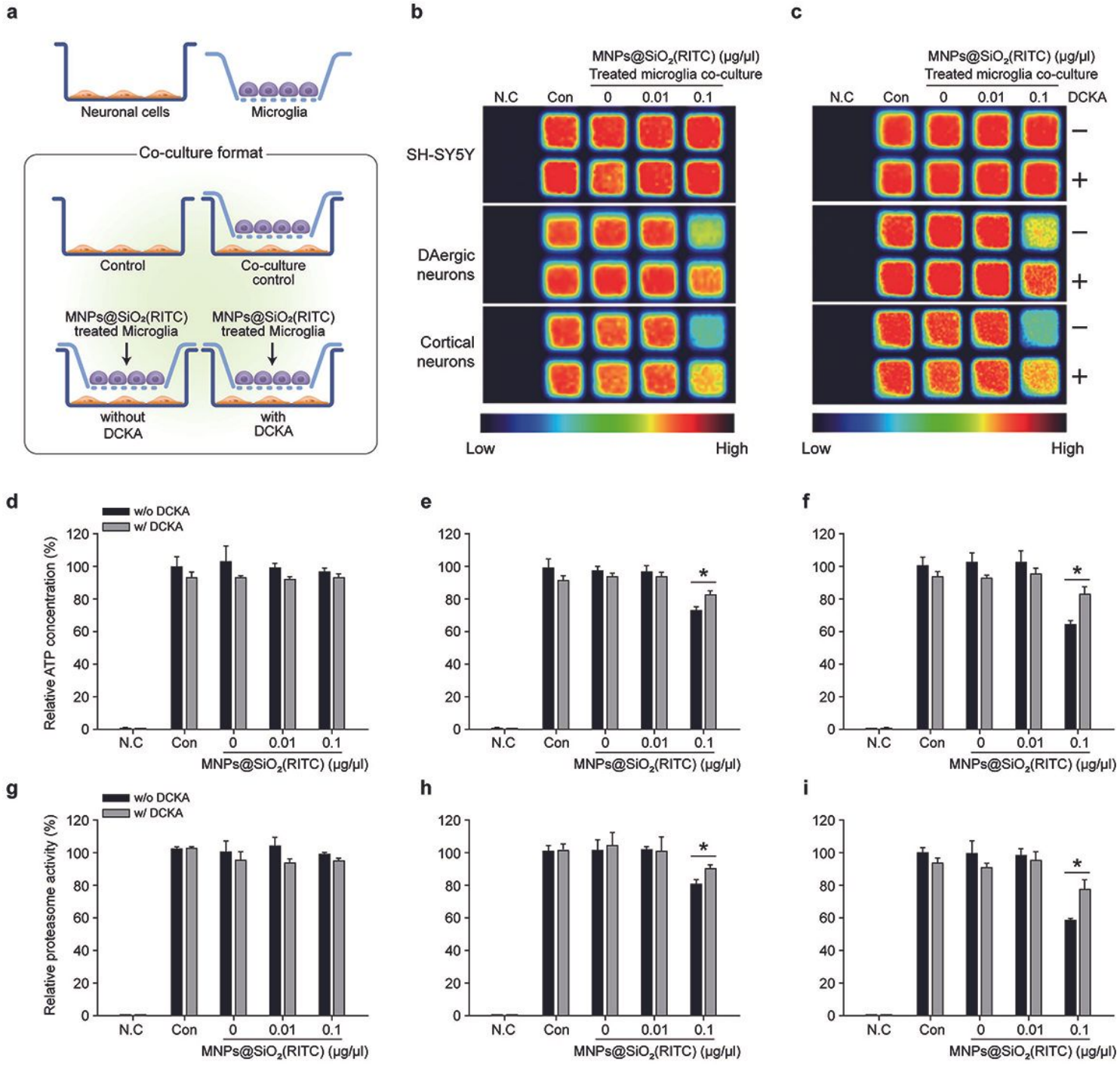


Figure 5

Evaluation of the intracellular ATP level and proteasomal activity in MNPs@SiO2(RITC)-treated microglia-cocultured neurons. a Schematic representation of the primary rat microglia and neuronal cell coculture system. Luminescence images of the ATP level b and proteasomal activity c. N.C.: non-treated control control; Con: neuronal cell only; DCKA: 5,7-dichlorokynurenic acid. Plus and minus signs indicate with or without DCKA treatment. Statistical analysis of ATP levels in d SH-SY5Y, e dopaminergic, and f cortical neurons. Statistical analysis of proteasomal activity in g SH-SY5Y, h dopaminergic, and i cortical neurons. *p < 0.05 vs. without DCKA.

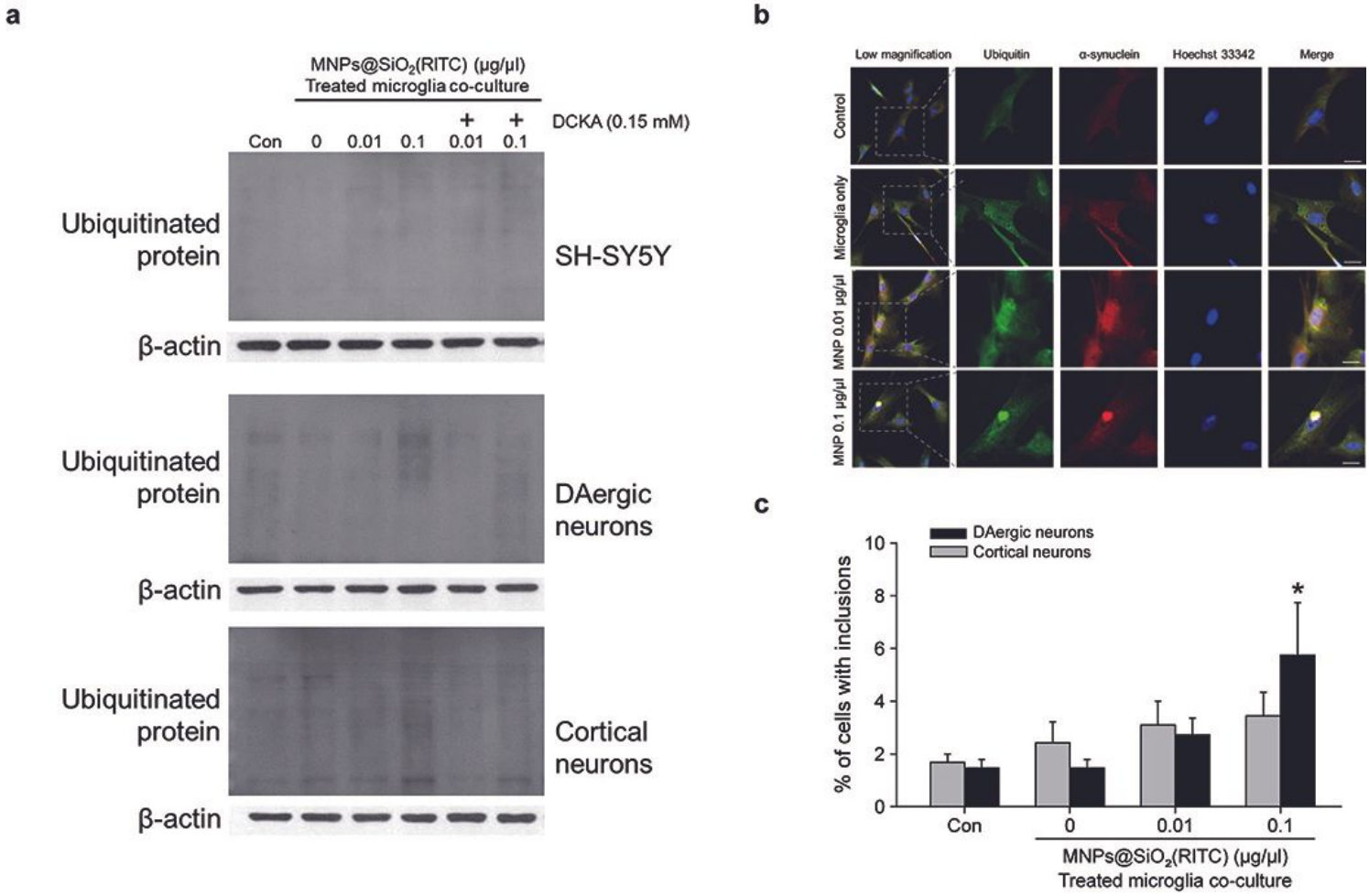


## Figure 6

Ubiquitinated proteins and inclusion bodies accumulate in MNPs@SiO2(RITC)-treated microglia-cocultured neurons. a Immunoblotting analysis of ubiquitinated proteins in the MNPs@SiO2(RITC)-treated microglia-cocultured neurons. b Inclusion body formation in MNPs@SiO2(RITC)-treated microglia-cocultured cortical neurons. Ubiquitin (green), α-synuclein (red), and nucleus (blue) were immunostained. Scale bar = 10 μm. c Quantification (%) of cells with inclusion bodies. *p < 0.05 vs. non-treated control.

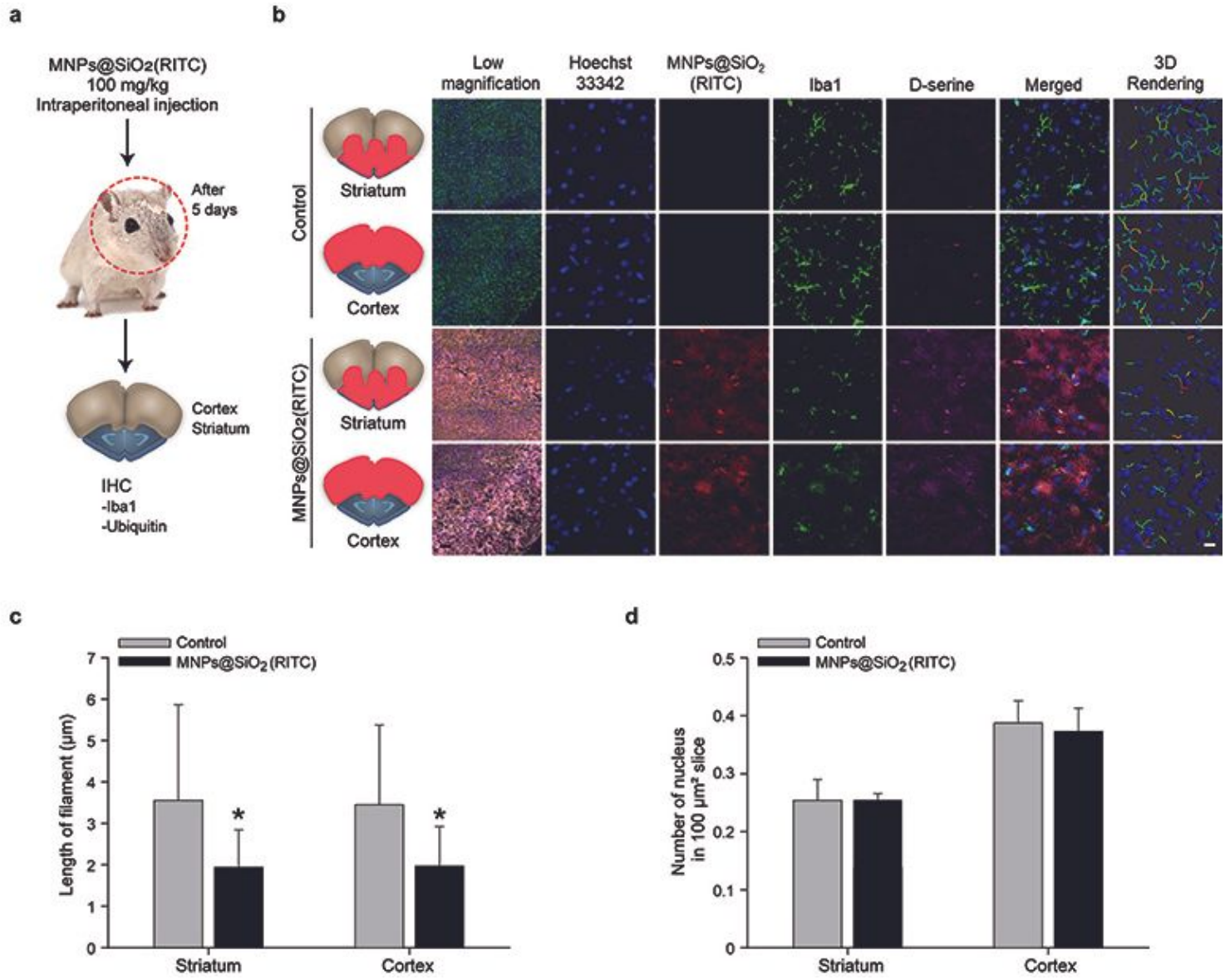


## Figure 7

Microglial activation and D-serine distribution in MNPs@SiO2(RITC)-treated mouse brains. a Schematic representation of the in vivo analysis. b Immunohistochemical analysis of the cerebellum regions of mice. Low-magnification images are merged with the florescence images of Hoechst 33342 (blue), MNPs@SiO2(RITC) (red), Iba1 (green), and D-serine (violet) to show region-specific structures and the distribution of MNPs@SiO2(RITC) and D-serine. Scale bar = 100 μm. Magnified images are separated into Hoechst 33342, MNPs@SiO2(RITC), Iba1, and D-serine and Iba1-based 3D-rendered images. White scale bar = 10 μm. c Filament length determined from the 3D-rendered images. d Quantification of nuclei in brain sections. *p < 0.05 vs. control.

# Supplementary Files

This is a list of supplementary files associated with this preprint. Click to download.

- AdditionalFile1.docx
- AdditionalFile10.pdf
- GraphicalAbstract.pdf
- AdditionalFile11.pdf
- AdditionalFile12.pdf
- AdditionalFile13.pdf
- AdditionalFile14.pdf
- AdditionalFile15.pdf
- AdditionalFile16.pdf
- AdditionalFile17.pdf
- AdditionalFile2.docx
- AdditionalFile3.docx
- AdditionalFile4.docx
- AdditionalFile5.docx
- AdditionalFile6.docx
- AdditionalFile7.pdf
- AdditionalFile8.pdf
- AdditionalFile9.pdf